PCCP

Accepted Manuscript

ROYAL SOCIETY OF CHEMISTRY

www.rsc.org/pccp

Journal Name

ARTICLE

Synergistic "Ping-Pong" Energy Transfer For Efficient Light Activation in a Chromophore-Catalyst Dyad

Received 00th January 20xx,
Accepted 00th January 20xx

DOI: 10.1039/x0xx00000x

www.rsc.org/

Annamaria Quaranta,*[a] Georgios Charalambidis,[b] Christian Herrero,[c] Sofia Margiola,[b] Winfried Leibl,[a] Athanassios Coutsolelos*[b] and Ally Aukauloo,*[a,c]

The synthesis of a porphyrin-Ru^{II}polypyridine complex where the porphyrin acts as the photoactive unit and the Ru^{II}polypyridine as the catalytic precursor is described. Comparatively, the free base porphyrin was found to outperform the ruthenium based chromophore in the yield of light induced electron transfer. Mechanistic insights indicate occurrence of a ping-pong energy transfer from the ^{1}LC excited state of the porphyrin chromophore to the ^{3}MCLT state of the catalyst and back to the ^{3}LC excited state of the porphyrin unit. The latter, triplet-triplet energy transfer back to the chromophore efficiently competes with fast radiationless deactivation of the excited state at the catalyst site. The energy thus recovered by the chromophore allows improved yield of formation of the oxidized form of the chromophore and concomitantly of the oxidation of the catalytic unit by intramolecular charge transfer. The presented results are among the rare examples where a porphyrin chromophore is successfully used to drive an oxidative activation process where reductive processes prevail in literature.

Introduction

Light-induced electron transfer processes in molecular assemblies constituting of a sensitizer covalently linked to a catalyst are determining steps in their functioning. These dyads are designed to harvest light energy to trigger electron transfer processes. The challenge is to accumulate charges at the catalytic unit to perform multi-electron catalysis.[1–3] Such a task is not a trivial pursuit. It demands among others the matching of the thermodynamic properties of the photoactivated chromophore with the redox properties of the catalytic unit. Another issue is to optimise the directional electron transfer while avoiding deleterious electron or energy transfer side reactions. The aims behind is to use light and renewable sources to perform catalysis in a sustainable fashion. Henceforth, the right selection of each constitutive component is of primary importance. A prominent chromophore that is still used as model compound in such supramolecular assemblies is the well documented $[Ru^{II}(bpy)_3]^{2+}$. A well-furnished literature is accessible with such chromophore.[4–13] On the catalytic side both reduction and oxidation reactions are under focus. Photocatalytic reduction reactions such as production of H_2 have been investigated quite successfully and to a lesser extent photo-oxidation reactions. This is mainly due to the scarcity of robust oxidative catalysts. Recently, Meyer *et al.* and other groups have developed mononuclear ruthenium based complexes as molecular catalysts performing the four-electron oxidation of water. From a synthetic point of view, it was of a less daunting task to covalently anchor a sensitizer to a catalytic unit such as $[Ru^{II}(tpy)(bpy)OH_2]^{2+}$ (tpy = 2,2':6',2''-terpyridine, bpy = 2,2'-bipyridine). Along this line, Rocha and coworkers[13] have reported on the photo-oxidation of various benzylic alcohols to the corresponding aldehydes through a two-electron oxidation process. Hamelin and coworkers[14,15] described the light-driven oxygen atom transfer reaction from the catalytic unit to sulphur organic substrates. More recently, Meyer has reported the photo-oxidation of water within such dyads.[16] With the target to decipher the intrinsic light activation pathways occurring in such dyads, we have recently shown[17] that the catalyst $[Ru^{II}(tpy)(bpy)OH_2]^{2+}$ could be activated either by an energy or electron transfer from a ruthenium trisbipyridine-related chromophore. We have clearly demonstrated that these processes were function of the substitution pattern on the bipyridine ligand on the chromophore. As such, these studies raise the issue that understanding the light activation pathways is essential to optimise the observed photocatalytic activity in such supramolecular assemblies. In this paper we investigate the activation of $[Ru^{II}(tpy)(bpy)Cl]^{+}$ through a covalently linked porphyrin. The interests for this family of sensitisers are multiple: [18–23]

[a] Service de Bioénergétique, Biologie Structurale et Mécanismes (SB_2SM), CEA, iBiTec-S ; Biochimie Biophysique et Biologie Structurale (B_3S), I_2BC, UMR 9198, F-91191 Gif-sur-Yvette, France. Email : annamaria.quaranta@cea.fr
[b] Department of Chemistry, University of Crete, Laboratory of Bioinorganic Chemistry, Voutes Campus, P.O. Box 2208, 71003, Heraklion, Crete, Greece. Email: coutsole@chemistry.uoc.gr
[c] Institut de Chimie Moléculaire et des Matériaux d'Orsay, UMR-CNRS 8182, Université Paris-Sud XI, F-91405 Orsay, France. Email : ally.aukauloo@u-psud.fr
Electronic Supplementary Information (ESI) available: [details of any supplementary information available should be included here]. See DOI: 10.1039/x0xx00000x

- the very strong absorption of the Soret band in the 400–450 nm region, as well as a significant absorption in the 500–700 nm region (Q-bands), makes porphyrin derivatives well adapted to efficiently absorb the solar emission spectrum; a high intersystem crossing quantum yield (0.88-0.90 in polar solvents) resulting in the formation of a long-lived triplet excited state (10-30 µs) makes it well-suited for interaction with electron donors and acceptors;
- synthetic handles at the *meso* and *beta* positions of the porphyrinic ring allows tailoring of the spectroscopic as well as electrochemical properties;
- porphyrins, not containing rare metals, are conveniently suited for large scale application.

In this work, the free base porphyrin was found to outperform the yield of light induced electron transfer in similar assemblies with ruthenium based chromophores in presence of an electron acceptor. Mechanistic insights indicate occurrence of a ping-pong energy transfer from the ^{1}LC excited state of the porphyrin chromophore to the ^{3}MCLT state of the catalyst and back to the ^{3}LC excited state of the porphyrin unit. The latter, triplet-triplet energy transfer back to the chromophore efficiently competes with fast radiation less deactivation of the excited state at the catalyst site. The energy thus recovered by the chromophore allows improved yield of formation of the oxidized form of the chromophore and concomitantly of the oxidation of the catalytic unit by intramolecular charge transfer. Such energy transfer processes have been evidenced in several multichromophoric systems leading to enhanced formation of long-lived triplet[24,25] or charge separate states[26,27] or were used for $^1O_2$ mediated photooxidation reaction.[28] The presented results are among the rare examples where a porphyrin chromophore is successfully used to drive an oxidative activation process where reductive processes prevail in literature.

Results and discussion

Synthetic procedures

The synthesis of the dyads presented in this paper is shown in Scheme 1. A two-step reaction was used for the synthesis of the terpyridine substituted porphyrin **H_2-P-terpy**. In the first step the carboxy-substituted terpyridine **terpy-COOH** was converted to the corresponding acyl chloride after refluxing in $SOCl_2$. Addition of amino porphyrin **H_2-P-NH_2**[29] and reflux in THF in the presence of Et_3N afforded **H_2-P-terpy**. The

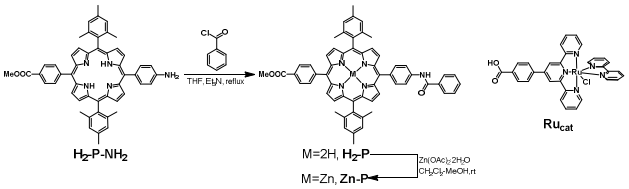

Scheme 1. Synthesis of dyads H2-P-Rucat and Zn-P-Rucat.

Scheme 2. Synthesis of the two reference chromophores (**H_2-P** and **Zn-P**) and the

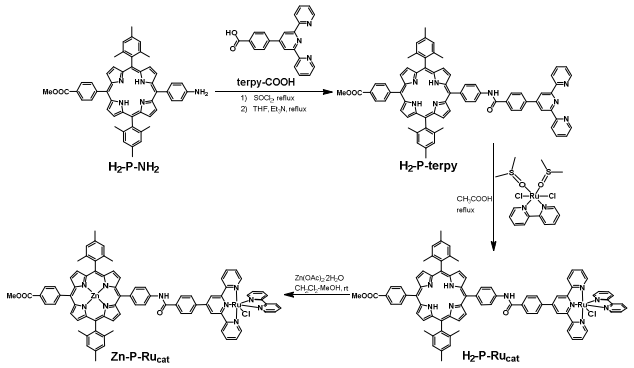

structure of reference catalyst **Ru_{cat}**.

free base dyad **H_2-P-Ru_{cat}** was prepared by refluxing **$Ru(bpy)(DMSO)_2Cl_2$**[30] and **H_2-P-terpy** in acetic acid. Finally metalation with zinc acetate yielded the second dyad **Zn-P-Ru_{cat}**. The synthesis of the two porphyrin reference compounds is shown in Scheme 2. Starting from amino porphyrin **H_2-P-NH_2** and after reflux with benzoyl chloride in THF and Et_3N, **H_2-P** was obtained. Metalation of the porphyrin ring with zinc acetate afforded the second reference compound **Zn-P**. All new compounds were fully characterized by NMR experiments (^{1}H and ^{13}C) and MALDI-TOF mass spectrometry.

Electrochemical and spectroscopic characterisation

Electrochemical properties of the dyads and reference compounds, investigated by cyclic and square-wave voltammetry, are reported in Table 1. For the dyad **H_2-P-Ru_{cat}** the observed electrochemical properties correspond to those obtained separately for the constitutive units **H_2-P** and **Ru_{cat}**. On the anodic side, waves at 0.93 V and 1.13 V correspond to the oxidation of **$Ru^{III}_{cat}/Ru^{II}_{cat}$** and **$H_2$-$P^+$/$H_2$-P** moieties respectively, while on the cathodic side peaks at -1.09 V and -1.23 V originate from reduction of the porphyrin and the bipyridine moieties. For the dyad **Zn-P-Ru_{cat}**, the first oxidation occurs at very similar potentials as those observed

Table 1. Electrochemical data

	$E_{1/2}$ (P^-/P^{2-})	$E_{1/2}$ (tpy^0/tpy^-)	$E_{1/2}$ (bpy^0/bpy^-)	$E_{1/2}$ (P/P^-)	$E_{1/2}$ (Ru^{III}/Ru^{II})	$E_{1/2}$ (P^+/P)	$E_{1/2}$ (P^{2+}/P^+)
Ru_{cat}		-1.42	-1.25		0.94		
H_2-P	-1.58			-1.08		1.14	1.42
Zn-P				-1.25		0.90	1.25
H_2-P-Ru_{cat}	-1.58	-1.42	-1.23	-1.09	0.93	1.13	1.37
Zn-P-Ru_{cat}		-1.41	-1.25	-1.25	0.93	0.93	1.22

$E_{1/2}$ = (E_{pa}+ E_{pc})/2 in Volts *vs* SCE, measured in benzonitrile, sweep rate= 100 mV/s.

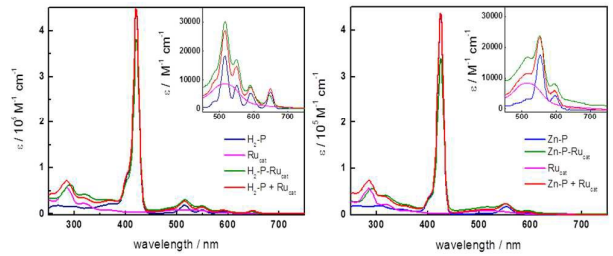

Figure 1. UV-vis absorption spectra for the dyads and the reference compounds. (Left) **H_2-P-Ru$_{cat}$**, (right) **Zn-P-Ru$_{cat}$** . Solvent was chloroform except for the **Ru$_{cat}$**. (in acetonitrile).

for each of the **ZnP** and **Ru$_{cat}$** components. This results in a two-electron oxidation wave observed at 0.93 V and similarly a two-electron reduction wave occurs at -1.25 V.

The electronic absorption spectra of the compounds in chloroform are shown in Figure 1. Reference compounds **H_2-P** (left) and **Zn-P** (right) exhibit typical porphyrin absorption features with an intense Soret band (421 nm for **H_2-P** and 425 nm for **Zn-P**) and moderate Q bands (516, 551, 591, 649 nm for **H_2-P** and 554, 597 nm for **Zn-P**). These features are present also in the dyads, accompanied by the characteristic MLCT (515 nm) and MC (320 nm) bands, originating from the **Ru$_{cat}$** unit. It appears that the individual features of the two moieties are not significantly altered in the dyads, although the Soret band is less intense in the dyads. This perturbation has previously been observed in similar systems.[31]

The excited states of the dyads **H_2-P-Ru$_{cat}$** and **Zn-P-Ru$_{cat}$** were characterised by steady-state emission and transient absorption spectroscopy and compared to reference compounds **H_2-P**, **Zn-P** and **Ru$_{cat}$**. Upon irradiation of **H_2-P-Ru$_{cat}$** at 590 nm, where 70% of incident light is absorbed by the **H_2-P** moiety, the resulting luminescence spectrum in chloroform (Figure S4 left, SI) shows bands at 655 nm and 715 nm, originating from the porphyrin fluorescence, and a small contribution on the 715 nm peak coming from the **Ru$_{cat}$** luminescence. However, the emission quantum yield is greatly reduced in the dyad (Φ_f = 0.0024, Table 2) as compared to the reference **H_2-P** (Φ_f = 0.118). These results suggest the presence of an intramolecular reaction (energy or electron transfer) responsible for the deactivation of the singlet excited state of the porphyrin. From the energetics point of view, the energy of ^{1}**H_2-P** excited state is not sufficient to drive reduction (ΔG = +450 mV)[‡] or oxidation (ΔG = +110 mV) of the attached ruthenium moiety. However the singlet excited state of the porphyrin and the triplet ^{3}MLCT of **Ru$_{cat}$** lie very close in energy (Table 2). Energy transfer between these two levels is normally spin-forbidden but, due to the strong spin-orbit coupling induced by the ruthenium heavy atom effect, this process is most likely responsible for the quenching of the porphyrin excited state. This mechanism has previously been observed in related porphyrin-ruthenium polypyridine dyads.[31,33,34] Upon irradiation at 532 nm, where only 40% of the incident light is absorbed by the **H_2-P** moiety, the fluorescence quantum yield accordingly decreases to Φ_f = 0.0012, suggesting that singlet-singlet energy transfer from Ru ^{1}MLCT excited state to the porphyrin singlet excited state does not operate because, otherwise, no decrease in Φ_f would be expected. Thus, steady-state fluorescence studies indicate that irradiation of the dyad results in the formation of a ^{3}MLCT excited state centred on the ruthenium. Further evolution of this state in the dyads will be presented below. In the isolated catalytic unit or in a **Ru-Ru$_{cat}$** assembly the ^{3}**Ru$_{cat}$*** state decays rapidly to the ground state (~300 ps at room temperature).[§] The fast excited state quenching on these Ru(tpy)(bpy) catalyst units represents a serious difficulty for its efficient activation by light.

Upon excitation of **H_2-P-Ru$_{cat}$** with a 532 nm laser pulse, only typical features of the porphyrin triplet excited state[35] were observed (Figure 2a), as obtained for the reference **H_2-P** under identical experimental conditions. The amplitude of ΔA in the dyad is about 60% of ΔA in the free-base porphyrin. However, formation of ^{3}**H_2-P** exclusively *via* intersystem crossing from the ^{1}**H_2-P** state should yield only ~35% of the triplet porphyrin (Φ_T).[§§] This suggests that also the short-lived ***Ru$_{cat}$** is involved in generating the ^{3}**H_2-P** species, most likely by triplet-triplet energy transfer, which is a downhill reaction (ΔG = -340 meV). The diminished lifetime of the triplet excited state of the **H_2-P-Ru$_{cat}$** dyad (2.5 µs) compared to the reference compound **H_2-P** (25 µs), is assigned to the presence of the heavy atom effect of the ruthenium which enhances the spin-orbit coupling interaction.[33,36] To sum up, light absorption in the **H_2-P-Ru$_{cat}$** dyad, absorbed either by the chromophore or the catalyst,

Table 2. Photophysical data for the different compounds studied

	Φ_f	λ_{em}/ nm	E_S/eV	Φ_{ISC}	E_T/eV	τ_T/ µs
Ru$_{cat}$	0.004	717		~1[a]	~1.85[b]	<0.01
H_2-P	0.118	655,714	1.91[c]	0.88[c]	1.51[d]	25
Zn-P	0.039	610,655	2.06[c]	0.90[c]	1.59[d]	12
H_2-P-Ru$_{cat}$	0.0024	655,714				2.5
Zn-P-Ru$_{cat}$	0.00062	610,655,750				1.9

[a] expected by analogy with $[Ru(bpy)_3]^{2+}$ and $[Ru(tpy)_2]^{2+}$; [b] estimated according to ref. [32](cf SI, Fig. S6); [c] 0-0 transition obtained from the intersection between normalised absorption and fluorescence spectra; [d]from maximum of phosphorescence at 77 K (cf SI, Fig. S7, S8).

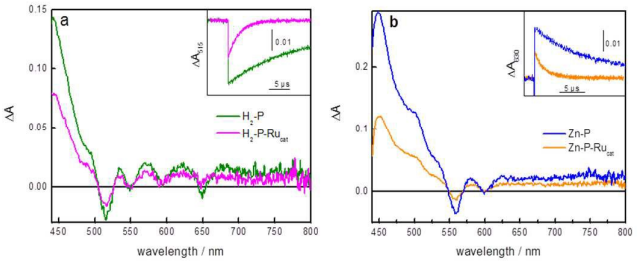

Figure 2. (a) Transient absorption spectra at 100 ns after laser flash for **H_2-P** (magenta) and **H_2-P-Ru$_{cat}$** (green); **(b) Zn$_2$-P** (blue) and **Zn-P-Ru$_{cat}$** (orange) in acetone/CH_3CN (50:50) argon-purged solutions. Excitation wavelength: 532 nm. Absorbance: 0.1. Laser energy: 9-10 mJ. Inset: kinetic traces at **(a)** 515 nm **(b)** and 630 nm.

ultimately results in the formation of a triplet excited state, mainly localized on **H_2-P** and having a lifetime of 2.5 µs (Scheme 3, left). These findings are in line with previous studies on the photophysical properties of porphyrin-ruthenium dyads.[31,33,37–40] In the case of the **Zn-P-Ru$_{cat}$** dyad, upon irradiation at 555 nm, where 85% light is absorbed by the **Zn-P** moiety, emission quantum yield is strongly decreased as compared to the reference porphyrin values. In addition, the emission spectrum exhibits, together with the porphyrin bands at 610 nm and 655 nm, a new broad band peaking at 750 nm (~1.65 eV), 35 nm red-shifted as compared to the **Ru$_{cat}$** emission (Fig. S4 right, SI), indicating the presence of a low-lying emitting excited state. This band was red-shifted and enhanced in more polar solvent (Fig. S5, SI). Decay from this excited state, possibly due to the formation of an intramolecular exciplex, which is stabilised in polar solvents, may prevent the formation of the triplet excited state. As in the case of the **H_2-P-Ru$_{cat}$** dyad, intramolecular electron transfer is endergonic for **Zn-P-Ru$_{cat}$** (ΔG = +120 mV) for either reduction or oxidation of the appended ruthenium moiety. Thus, in this case, quenching of the porphyrin singlet excited state may occur either by singlet-triplet energy transfer, which is thermodynamically favourable, or *via* the formation of an exciplex, which lies close (~1.65 eV in chloroform, ~1.59 eV in acetonitrile/acetone mixture)[§§§] to the porphyrin triplet excited state.

Upon irradiation of the **Zn-P-Ru$_{cat}$** dyad at 532 nm, the porphyrin unit absorbs 60% of light and the calculated fluorescence quantum yield is accordingly slightly lower (Φ_f = 5.6 x 10^{-4}). Excitation with a laser pulse, as in the case of the **H_2-P-Ru$_{cat}$** dyad, resulted in the formation of the porphyrin triplet excited state (Figure 2b) with a ΔA being ~50% that of the reference **Zn-P** and no other intermediate detected, suggesting that intersystem crossing from ^{1}**Zn-P*** excited state might be the only pathway to generate ^{3}**Zn-P***. In conclusion, light absorption in the **Zn-P-Ru$_{cat}$** dyad results in the formation of a triplet excited state mainly localized on **Zn-P** and having a lifetime of 1.9 µs. The different deactivation pathways in both dyads are summarized in Scheme 3.

Photoinduced electron transfer

Having assessed that light absorption ultimately produces in both dyads a porphyrin triplet excited state lasting about 2 µs, we studied the reactions initiated in the presence of a reversible electron acceptor (methyl viologen, MV^{2+}) in order to investigate the possibility to oxidise **Ru$_{cat}$** by an

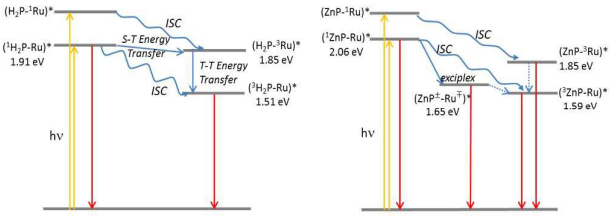

Scheme 3. Energy scheme for intramolecular reactions within the dyads **H_2-P-Ru$_{cat}$** (left) and **Zn-P-Ru$_{cat}$** (right). Yellow arrows, light absorption; red arrows, emission; blue arrows, intramolecular transitions.

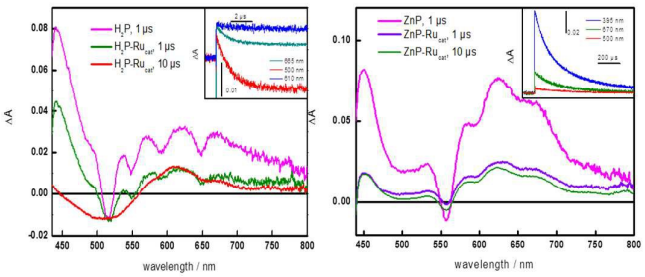

Figure 3. Left: differential absorption spectra of acetone:CH_3CN (50:50) solutions of **H_2-P-Ru$_{cat}$** and **H_2-P** in the presence of 10 mM MV^{2+} (inset: kinetics at 500, 610 and 665 500 and 670 nm). Right: **Zn-P-Ru$_{cat}$** and **Zn-P** in the presence of 10 mM MV^{2+} (inset: kinetics at 395, nm).

intramolecular electron transfer reaction. In both dyads, excited at 532 nm, the triplet state was quenched by MV^{2+} with a rate constant close to diffusion limit (~10^9 M^{-1} s^{-1}). The transient spectra recorded 1 µs after the laser pulse (Figure 3) indicate the formation of the radical ion pair $MV^{\bullet+}$ (positive absorption bands at 400 nm and 610 nm) and **H_2-P$^{\bullet+}$-Ru$_{cat}$** or **Zn-P$^{\bullet+}$-Ru$_{cat}$** respectively (broad positive absorption band between 500 and 800 nm, on which negative bands due to the ground state depletion of the Q bands are superimposed). These spectral characteristics match well those observed with the reference porphyrins **H_2-P$^{\bullet+}$** or **Zn-P$^{\bullet+}$** and are consistent with the literature.[41,42] However, after the initial formation of the porphyrin radical cation, a different behaviour was observed for the two dyads. In the case of **H_2-P-Ru$_{cat}$**, the **H_2-P$^{\bullet+}$** initially formed, evolved in 1.5 µs (Fig. 3, inset, kinetics at 665 nm and 500 nm) to yield the formation of **Ru$^{III}_{cat}$** characterised by the depletion of the absorption band between 400 nm and 560 nm[17] (spectrum at 10 µs), while the absorption due to $MV^{\bullet+}$ (610 nm, inset) was only slightly decreased. Subsequent charge recombination between $MV^{\bullet+}$ and **Ru$^{III}_{cat}$** occurred in ~200 µs. In contrast, in the case of **Zn-P-Ru$_{cat}$**, once the $MV^{\bullet+}$ and **Zn-P$^{\bullet+}$** radical species were formed (Fig. 3, right), only charge recombination in 200 µs (inset) without distinguishable formation of **Ru$^{III}_{cat}$** was observed. The difference between the two dyads is rationalised by considering their different electrochemical properties. Due to the higher oxidation potential of the P^+/P couple in the dyad **H_2-P-Ru$_{cat}$** a driving force ΔG = -200 mV is available for **H_2-P$^{\bullet+}$** to oxidise **Ru$^{II}_{cat}$**, whereas in the dyad **Zn-P-Ru$_{cat}$** the available driving force for **Zn-P$^{\bullet+}$** to oxidise **Ru$^{II}_{cat}$** is close to zero (Table 1) and therefore an equilibrium is expected to be established between **Zn-P$^{\bullet+}$** and **Ru$^{III}_{cat}$**.

Conclusions

The photophysical studies presented here indicate that in both dyads, excitation of either chromophore, results in efficient formation of a triplet excited state centred on the porphyrin moiety. The interesting fact that the triplet excited state on the porphyrin chromophore unit lies lower in energy than the

triplet excited state on the ruthenium catalytic unit, allows back transfer to the chromophore of excitation energy which would otherwise be lost by rapid quenching on the catalyst. This triplet has a lifetime of ~2 µs that can be intercepted by an electron acceptor. However, in the dyad **Zn-P-Ru$_{cat}$**, the metallated porphyrin radical cation lacks the driving force to oxidise **Ru$_{cat}$**, while in the dyad **H$_2$-P-Ru$_{cat}$** the free–base porphyrin radical cation is able to trigger the first step in the catalytic cycle of **Ru$^{II}_{cat}$** generating the **Ru$^{III}_{cat}$** species. Moreover, for the latter dyad, the photo-induced oxidation of **Ru$_{cat}$** seems to be very efficient. Using $\Delta\varepsilon$ ~ -10000 M^{-1} cm^{-1} for **Ru$_{cat}$** and $\Delta\varepsilon$ ~ 3000 M^{-1} cm^{-1} nm for the **MV$^{\bullet+}$** at 500 nm[43] once **H$_2$-P$^{\bullet+}$** signal has disappeared; and $\Delta\varepsilon$ ~ 600 M^{-1} cm^{-1} at 775 nm for **MV$^{\bullet+}$** (and $\Delta\varepsilon$ ~ 0 for **Ru$_{cat}$** and **H$_2$-P$^{\bullet+}$**) at initial time, it results that ~2.0 µM **MV$^{\bullet+}$** initially generated are converted into ~2.3 µM **Ru$^{III}_{cat}$**. Considering the uncertainties in the extinction coefficients this indicates a yield close to unity. For comparison, in the case of the **Ru$_{chr}$-Ru$_{cat}$** dyad previously investigated, the yield could be estimated to be roughly 0.3. Interestingly, another aspect by which the **H$_2$-P-Ru$_{cat}$** dyad compares favourably to our previously reported **Ru$_{chr}$-Ru$_{cat}$** system, in that **Ru$_{cat}$** oxidation (~1.5 µs) is about one order of magnitude faster than in **Ru$_{chr}$-Ru$_{cat}$** (~20 µs) despite the fact that the driving force is more favourable (ΔG= -700 mV *vs* -200 meV in the latter system. This suggests that kinetic factors are also important for the efficiency of oxidation of the catalytic site. Hence, our findings suggest that porphyrins chromophores can be valid alternative to $[Ru(bpy)_3]^{2+}$ for efficient collection and conversion of light into oxidative power for the development of molecular models in artificial photosynthesis.

Acknowledgements

Financial support from the COST action CM1202 "PERSPECT-H2O" is gratefully acknowledged. This work was supported by, the French Infrastructure for Integrated Structural Biology (FRISBI) ANR-10-INSB-05-01, the Labex CHARMMMAT, the European Commision FP7-REGPOT-2008-1, Project BIOSOLENUTI No 229927 and the Greek General Secretariat for Research and Technology.

Experimental

Materials. Compounds **terpy-COOH**,[44] **H$_2$-P-NH$_2$**,[29] **Ru(bpy)(DMSO)$_2$Cl$_2$**,[30] and **Ru$_{cat}$**[45] were prepared according to published procedures. Tetrahydrofuran was freshly distilled from Na/benzophenone. All other chemicals and solvents were purchased from commercial sources and used as received.

NMR Spectra. NMR spectra were recorded on Bruker AVANCE III-500 MHz and Bruker DPX-300 MHz spectrometers using solutions in deuterated solvents and the solvent peak was chosen as the internal standard.

Mass Spectra. High-resolution mass spectra were obtained on a Bruker UltrafleXtreme matrix assisted laser desorption ionization time-of-flight (MALDI-TOF) spectrometer using trans-2-[3-(4-tert-butylphenyl)-2-methyl-2-propenylidene]malononitrile (DCTB) as matrix.

Electrochemistry. Cyclic and square wave voltammetry experiments were carried out at room temperature using an AutoLab PGSTAT20 potentiostat and appropriate routines available in the operating software (GPES version 4.9). All measurements were carried out in freshly distilled and deoxygenated benzonitrile with a solute concentration of *ca*. 1.0 mM in the presence of tetrabutylammonium tetrafluoroborate (0.1 M) as supporting electrolyte, at a scan rate of 100 mV s^{-1}. A three-electrode cell setup was used with a platinum working electrode, a saturated calomel (SCE) reference electrode, and a platinum wire as counter electrode. In all measurements the ferrocene/ferrocenium couple was at 0.56 V versus SCE under the above conditions.

Spectroscopy. Ground state absorption spectra were measured either on a Shimadzu UV-1700 or an Analytic Jena Specord210 spectrophotometer. Steady-state emission spectra were obtained exciting **H$_2$-P** and **H$_2$-P-Ru$_{cat}$** at 590 nm and **Zn-P** and **Zn-P-Ru$_{cat}$** at 555 nm using a JASCO FP-6500 fluorescence spectrophotometer equipped with a red-sensitive WRE-343 photomultiplier tube (wavelength range 200–850 nm). Fluorescence quantum yields were calculated in chloroform from corrected emission spectra following the standard methods[46] using 5,10,15,20-tetraphenylporphyrin (Φ_f = 0.11 in toluene),[47] and 5,10,15,20-tetraphenylporphyrinato zinc (Φ_f = 0.03 in toluene)[47] as references. Low temperature phosphorescence spectra were measured in an ethanol:methanol (4:1) rigid matrix at 77 K using a Hitachi F-4500 spectrofluorimeter equipped with a liquid nitrogen sample holder. All transient absorption experiments were performed on an Edinburgh Instruments LP920 Flash Photolysis Spectrometer system incorporating a Continuum Q-switched Nd:YAG laser operating at 532 nm. The LP920 system is equipped with a 450 W Xenon arc lamp as the probe for the transient absorption measurements. In the time range 10 ns to 100 µs, the Xenon arc lamp was pulsed. Detection in the LP920 system is performed either via a Czerny-Turner blazed 500 nm monochromator (bandwidth: 1-5 nm) coupled with a Hamamatsu R928 photomultiplier tube (kinetics mode), or via a 500 nm blazed spectrograph (bandwidth: 5 nm) coupled with a water-cooled ICCD nanosecond Andor DH720 camera (spectral mode). Samples, having absorbances of ~0.1 at the excitation wavelength, were purged with argon prior to each experiment.

Synthesis

H$_2$-P-terpy. 4-([2,2':6', 2''-terpyridin]-4'-yl)benzoic acid (**terpy-COOH**) (75 mg, 0.21 mmol) was dissolved in $SOCl_2$ (2.8 mL) and stirred under an argon atmosphere at 80 °C for 2 h. $SOCl_2$ was removed under reduced pressure and the resulting acyl chloride terpyridine was dried under high vacuum at 50 °C for 1 h. The resulting solid was dissolved in anhydrous THF (9 mL) and anhydrous triethylamine (0.1 mL) and **H$_2$-P-NH$_2$** (55 mg,

0.07 mmol) were added. The reaction mixture was heated under argon at 70 °C overnight. The solvent was removed under reduced pressure, $CHCl_3$ (80 mL) was added and the mixture washed with water (3 x 50 mL). The organic layer was dried with Na_2SO_4, filtered and concentrated. The desired compound was isolated using silica column chromatography CH_2Cl_2:MeOH (100:6) to obtain **H_2-P-terpy** as a purple solid (72 mg, 91%). ^{1}H NMR (500MHz, $CDCl_3$): δ 8.87 (d, *J* = 4.7 Hz, 2H), 8.85 (s, 2H), 8.78 (m, 2H), 8.73 (m, 8H), 8.42 (d, *J* = 8.4 Hz, 2H), 8.36 (s, 1H), 8.31 (d, *J* = 8.4 Hz, 2H), 8.25 (d, *J* = 8.5 Hz, 2H), 8.20 (d, *J* = 8.5 Hz, 2H), 8.13 (d, *J* = 8.5 Hz, 2H), 8.10 (d, *J* = 8.5 Hz, 2H), 7.93 (dt, J_1 = 7.7 Hz, J_2 = 1.8 Hz, 2H), 7.41 (m, 2H), 7.29 (s, 4H), 4.11 (s, 3H), 2.64 (s, 6H), 1.85 (s, 12H), –2.60 (s, 2H). ^{13}C NMR (75 MHz, $CDCl_3$): δ 167.5, 165.7, 156.3, 156.1, 149.3, 147.1, 142.3, 139.5, 138.5, 138.4, 138.0, 137.9, 137.3, 135.5, 135.3, 134.7, 131.1, 131.0, 130.5, 129.6, 128.0, 127.9, 124.2, 121.7, 119.2, 118.8, 118.7, 117.9, 52.5, 21.8, 21.6. HRMS (MALDI-TOF) calcd. for $C_{74}H_{58}N_8O_3$ $[M]^+$ 1106.4632, found 1106.4628.

H_2-P-Ru$_{cat}$. Ruthenium complex (**Ru(bpy)(DMSO)$_2$Cl$_2$)** (55 mg, 0.11 mmol) was added to a solution of **H_2-P-terpy** (75 mg, 0.07 mmol) in acetic acid (30 mL) and the mixture was stirred under nitrogen at 100 °C overnight. After removing the solvent, the product was purified by column chromatography on silica CH_2Cl_2:MeOH (100:7) giving **H_2-P-Ru$_{cat}$** as a purple solid (70 mg, 74%). ^{1}H NMR (500MHz, $CDCl_3$): δ 11.15 (br s, 1H), 10.36 (s, 1H), 8.89 (d, *J* = 3.5 Hz, 2H), 8.83 (br s, 2H), 8.73 (d, *J* = 4.5 Hz, 2H), 8.68 (d, *J* = 4.5 Hz, 4H), 8.64 (d, *J* = 4.5 Hz, 2H), 8.52 (d, *J* = 6.5 Hz, 2H), 8.42 (d, *J* = 7.9 Hz, 4H), 8.30 (d, *J* = 7.9 Hz, 3H), 8.19 (br s, 2H), 8.08 (d, *J* = 6.5 Hz, 2H), 7.96 (br s, 2H), 7.75 (br s, 1H), 7.47 (br s, 4H), 7.30 (br s, 1H), 7.22 (s, 4H), 7.15 (br s, 1H), 7.05 (br s, 2H), 6.78 (br s, 1H), 4.10 (s, 3H), 2.56 (s, 6H), 1.78 (s, 12H), –2.61 (s, 2H). ^{13}C NMR (125 MHz, $CDCl_3$): 167.5, 167.2, 158.7, 158.3, 157.8, 155.9, 152.8, 151.5, 147.0, 144.0, 139.5, 139.4, 138.4, 137.9, 137.3, 137.0, 136.5, 135.4, 135.2, 134.7, 131.2, 129.6, 129.5, 128.1, 127.9, 127.5, 127.2, 126.8, 126.6, 125.1, 123.3, 120.0, 119.9, 119.2, 118.6, 117.8, 52.6, 21.8, 21.6. HRMS (MALDI-TOF) calcd for $C_{84}H_{66}Cl_2N_{10}O_3Ru$ $[M\text{-}Cl]^+$ 1399.4051, found 1399.4077.

Zn-P-Ru$_{cat}$. To a stirred solution of **H_2-P-Ru$_{cat}$** (30 mg, 0.02 mmol) in CH_2Cl_2 (15 mL) and MeOH (3 mL) zinc acetate dihydrate (85 mg, 0.39 mmol) was added. The reaction mixture was stirred at room temperature overnight. The solvent was removed in a rotary evaporator and the desired compound was isolated by silica column chromatography CH_2Cl_2:MeOH (100:8) to obtain **Zn-P-Ru$_{cat}$** as a purple solid (29 mg, 93%). ^{1}H NMR (500MHz, (DMSO-d_6): δ 10.93 (s, 1H), 10.14 (d, *J* = 5.1 Hz, 1H), 9.35 (s, 2H), 9.04 (d, *J* = 8.1 Hz, 2H), 8.96 (d, *J* = 8.2 Hz, 1H), 8.83 (d, *J* = 4.4 Hz, 2H), 8.71 (d, *J* = 4.4 Hz, 2H), 8.68 (d, *J* = 8.5 Hz, 1H), 8.61 (m, 6H), 8.46 (d, *J* = 8.0 Hz, 2H), 8.36 (m, 5H), 8.31 (d, *J* = 8.0 Hz, 2H), 8.23 (d, *J* = 8.0 Hz, 2H), 8.09 (m, 3H), 7.81 (t, *J* = 7.5 Hz, 1H), 7.67 (d, *J* = 5.4 Hz, 2H), 7.48 (d, *J* = 6.0 Hz, 1H), 7.43 (t, *J* = 6.5 Hz, 2H), 7.33 (s, 4H), 7.11 (t, *J* = 6.5 Hz, 1H), 4.04 (s, 3H), 2.59 (s, 6H), 1.80 (s, 12H). ^{13}C NMR (125 MHz, DMSO-d_6): 166.5, 135.3, 158.6, 158.3, 158.0, 155.6, 152.0, 151.9, 149.4, 149.1, 149.0, 148.7, 147.8, 143.8, 139.3, 139.1, 138.6, 138.4, 138.0, 137.0, 136.9, 136.0, 135.7, 134.5, 134.4, 132.1, 131.6, 130.4, 130.2, 129.4, 128.8, 128.6, 127.6, 127.3, 127.0, 126.5, 124.2, 123.8, 123.6, 120.2, 119.8, 118.5, 118.2, 118.0, 52.4, 21.4, 21.0. HRMS (MALDI-TOF) calcd. for $C_{84}H_{64}ClN_{10}O_3RuZn$ $[M\text{-}Cl]^+$ 1461.3186, found 1461.3171.

H_2-P. Benzoyl chloride (32 µL, 0.27 mmol) and **H_2-P-NH$_2$** (35 mg, 0.05 mmol) were dissolved in dry THF (4 mL) and dry triethylamine (50 µL) and the reaction stirred under argon at 70 °C overnight. At this time the solvent was removed under reduced pressure and the desired product was isolated by silica column chromatography CH_2Cl_2:EtOH (98:2) to obtain the desired product as a purple solid (31 mg, 78%). ^{1}H NMR (500MHz, $CDCl_3$): δ 8.86 (d, *J* = 4.7 Hz, 2H), 8.74 (d, *J* = 4.7 Hz, 2H), 8.72 (m, 4H), 8.43 (d, *J* = 8.4 Hz, 2H), 8.32 (d, *J* = 8.4 Hz, 2H), 8.25 (d, *J* = 8.5 Hz, 2H), 8.18 (s, 1H), 8.05 (m, 4H), 7.63 (m, 3H), 7.29 (s, 4H), 4.11 (s, 3H), 2.64 (s, 6H), 1.85 (s, 12H), –2.61 (s, 2H). ^{13}C NMR (75 MHz, $CDCl_3$): 167.5, 166.2, 147.0, 139.5, 138.5, 138.3, 138.0, 137.8, 135.3, 135.2, 134.7, 132.3, 131.2, 131.0, 130.4, 129.6, 129.1, 128.0, 127.9, 127.3, 119.2, 118.7, 118.5, 117.9, 52.6, 21.8, 21.6. HRMS (MALDI-TOF) calcd for $C_{59}H_{49}N_5O_3$ $[M]^+$ 875.3835, found 875.3841.

Zn-P. A mixture of **H_2-P** (27 mg, 0.03 mmol) and zinc acetate dihydrate (67 mg, 0.30 mmol) in CH_2Cl_2 (8 mL) and MeOH (2 mL) was stirred at room temperature overnight. The solvent was removed in a rotary evaporator and the desired compound was isolated by silica column chromatography CH_2Cl_2:EtOH (98:2) to obtain **Zn-P** as a brown solid (26 mg, 92%). ^{1}H NMR (500MHz, $CDCl_3$): δ 8.94 (d, *J* = 4.6 Hz, 2H), 8.82 (d, *J* = 4.6 Hz, 2H), 8.79 (m, 4H), 8.42 (d, *J* = 8.0 Hz, 2H), 8.32 (d, *J* = 8.0 Hz, 2H), 8.25 (d, *J* = 8.1 Hz, 2H), 8.16 (s, 1H), 8.03 (d, *J* = 7.4 Hz, 4H), 7.61 (m, 3H), 7.28 (s, 4H), 4.10 (s, 3H), 2.63 (s, 6H), 1.83 (s, 12H). The ^{13}C-NMR spectrum could not be recorded due to the limited solubility in $CDCl_3$. HRMS (MALDI-TOF) calcd. for $C_{59}H_{47}N_5O_3Zn$ $[M]^+$ 937.2970, found 937.2963.

Notes and references

‡ $\Delta G = E_{ox}\text{-}E_{red}\text{-}E_{00}$

§ Minh-Huong Ha Thi, personal communication

§§ $\Phi_T = \Phi_{abs}$(**H_2-P**)·Φ_{ISC}(**H_2-P**)

§§§ From peak of the exciplex emission

1 J. H. Alstrum-Acevedo, M. K. Brennaman and T. J. Meyer, *Inorg. Chem.*, 2005, **44**, 6802–6827.

2 C. Herrero, A. Quaranta, W. Leibl, A. W. Rutherford and A. Aukauloo, *Energy Environ. Sci.*, 2011, **4**, 2353–2365.

3 M. D. Kärkäs, O. Verho, E. V. Johnston and B. Åkermark, *Chem. Rev.*, 2014, **114**, 11863–12001.

4 N. Kaveevivitchai, R. Chitta, R. Zong, M. El Ojaimi and R. P. Thummel, *J. Am. Chem. Soc.*, 2012, **134**, 10721–10724.

5 T.-T. Li, F.-M. Li, W.-L. Zhao, Y.-H. Tian, Y. Chen, R. Cai and W.-F. Fu, *Inorg. Chem.*, 2015, **54**, 183–191.

6 C. Herrero, J. L. Hughes, A. Quaranta, N. Cox, A. W. Rutherford, W. Leibl and A. Aukauloo, *Chem. Commun.*, 2010, **46**, 7605–7607.

7 C. Herrero, A. Quaranta, S. Protti, W. Leibl, A. W. Rutherford, R. Fallahpour, M. F. Charlot and A. Aukauloo, *Chem.- Asian J.*, 2011, **6**, 1335–1339.

8 F. Li, Y. Jiang, B. Zhang, F. Huang, Y. Gao and L. Sun, *Angew. Chem. Int. Ed.*, 2012, **51**, 2417–2420.

9 D. L. Ashford, D. J. Stewart, C. R. Glasson, R. A. Binstead, D. P. Harrison, M. R. Norris, J. J. Concepcion, Z. Fang, J. L. Templeton and T. J. Meyer, *Inorg. Chem.*, 2012, **51**, 6428–6430.
10 M. R. Norris, J. J. Concepcion, D. P. Harrison, R. A. Binstead, D. L. Ashford, Z. Fang, J. L. Templeton and T. J. Meyer, *J. Am. Chem. Soc.*, 2013, **135**, 2080–2083.
11 E. A. Karlsson, B.-L. Lee, R.-Z. Liao, T. Åkermark, M. D. Kärkäs, V. S. Becerril, P. E. M. Siegbahn, X. Zou, M. Abrahamsson and B. Åkermark, *ChemPlusChem*, 2014, **79**, 936–950.
12 J. A. Treadway, J. A. Moss and T. J. Meyer, *Inorg. Chem.*, 1999, **38**, 4386–+.
13 W. Chen, F. N. Rein, B. L. Scott and R. C. Rocha, *Chem.- Eur. J.*, 2011, **17**, 5595–5604.
14 O. Hamelin, P. Guillo, F. Loiseau, M.-F. Boissonnet and S. Ménage, *Inorg. Chem.*, 2011, **50**, 7952–7954.
15 P. Guillo, O. Hamelin, P. Batat, G. Jonusauskas, N. D. McClenaghan and S. Menage, *Inorg. Chem.*, 2012, **51**, 2222–2230.
16 J. J. Concepcion, J. W. Jurss, M. R. Norris, Z. Chen, J. L. Templeton and T. J. Meyer, *Inorg. Chem.*, 2010, **49**, 1277–1279.
17 C. Herrero, A. Quaranta, R.-A. Fallahpour, W. Leibl and A. Aukauloo, *J. Phys. Chem. C*, 2013, **117**, 9605–9612.
18 L.-L. Li and E. W.-G. Diau, *Chem. Soc. Rev.*, 2012, **42**, 291–304.
19 M. E. El-Khouly, C. A. Wijesinghe, V. N. Nesterov, M. E. Zandler, S. Fukuzumi and F. D'Souza, *Chem. – Eur. J.*, 2012, **18**, 13844–13853.
20 M. Wasielewski, *Chem. Rev.*, 1992, **92**, 435–461.
21 F. D'Souza and O. Ito, *Coord. Chem. Rev.*, 2005, **249**, 1410–1422.
22 M. K. Panda, K. Ladomenou and A. G. Coutsolelos, *Coord. Chem. Rev.*, 2012, **256**, 2601–2627.
23 G. de la Torre, G. Bottari, M. Sekita, A. Hausmann, D. M. Guldi and T. Torres, *Chem. Soc. Rev.*, 2013, **42**, 8049–8105.
24 M. T. Whited, P. I. Djurovich, S. T. Roberts, A. C. Durrell, C. W. Schlenker, S. E. Bradforth and M. E. Thompson, *J. Am. Chem. Soc.*, 2011, **133**, 88–96.
25 F. N. Castellano, *Acc. Chem. Res.*, 2015, **48**, 828–839.
26 J. E. Yarnell, J. C. Deaton, C. E. McCusker and F. N. Castellano, *Inorg. Chem.*, 2011, **50**, 7820–7830.
27 T. Lazarides, T. M. McCormick, K. C. Wilson, S. Lee, D. W. McCamant and R. Eisenberg, *J. Am. Chem. Soc.*, 2011, **133**, 350–364.
28 C. Zhang, J. Zhao, S. Wu, Z. Wang, W. Wu, J. Ma, S. Guo and L. Huang, *J. Am. Chem. Soc.*, 2013, **135**, 10566–10578.
29 G. E. Zervaki, E. Papastamatakis, P. A. Angaridis, V. Nikolaou, M. Singh, R. Kurchania, T. N. Kitsopoulos, G. D. Sharma and A. G. Coutsolelos, *Eur. J. Inorg. Chem.*, 2014, **2014**, 1020–1033.
30 L. Tong, A. K. Inge, L. Duan, L. Wang, X. Zou and L. Sun, *Inorg. Chem.*, 2013, **52**, 2505–2518.
31 A. C. Benniston, G. M. Chapman, A. Harriman and M. Mehrabi, *J. Phys. Chem. A*, 2004, **108**, 9026–9036.
32 V. Grosshenny, A. Harriman, F. M. Romero and R. Ziessel, *J. Phys. Chem.*, 1996, **100**, 17472–17484.
33 L. Flamigni, N. Armaroli, F. Barigelletti, V. Balzani, J.-P. Collin, J.-O. Dalbavie, V. Heitz and J.-P. Sauvage, *J. Phys. Chem. B*, 1997, **101**, 5936–5943.
34 L. Flamigni, F. Barigelletti, N. Armaroli, J.-P. Collin, J.-P. Sauvage and J. A. G. Williams, *Chem. – Eur. J.*, 1998, **4**, 1744–1754.
35 L. Pekkarinen and H. Linschitz, *J. Am. Chem. Soc.*, 1960, **82**, 2407–2411.
36 A. C. Benniston, A. Harriman, C. Pariani and C. A. Sams, *Phys. Chem. Chem. Phys.*, 2006, **8**, 2051–2057.
37 A. Harriman, M. Hissler, O. Trompette and R. Ziessel, *J. Am. Chem. Soc.*, 1999, **121**, 2516–2525.
38 L. Flamigni, F. Barigelletti, N. Armaroli, J.-P. Collin, I. M. Dixon, J.-P. Sauvage and J. A. G. Williams, *Coord. Chem. Rev.*, 1999, **190–192**, 671–682.
39 A. C. Benniston, *Phys. Chem. Chem. Phys.*, 2007, **9**, 5739–5747.
40 L. Flamigni, F. Barigelletti, N. Armaroli, B. Ventura, J.-P. Collin, J.-P. Sauvage and J. A. G. Williams, *Inorg. Chem.*, 1999, **38**, 661–667.
41 Z. Gasyna, W. R. Browett and M. J. Stillman, *Inorg. Chem.*, 1985, **24**, 2440–2447.
42 J. Fajer, D. C. Borg, A. Forman, D. Dolphin and R. H. Felton, *J. Am. Chem. Soc.*, 1970, **92**, 3451–3459.
43 M. Montalti, A. Credi, L. Prodi, M. T. Gandolfi *Handbook of Photochemistry, Third Edition*, CRC Press, Boca Raton, FL, 2006.
44 E. C. Constable, E. L. Dunphy, C. E. Housecroft, M. Neuburger, S. Schaffner, F. Schaper and S. R. Batten, *Dalton Trans.*, 2007, 4323–4332.
45 N. Kaveevivitchai, R. Zong, H.-W. Tseng, R. Chitta and R. P. Thummel, *Inorg. Chem.*, 2012, **51**, 2930–2939.
46 G. A. Crosby and J. N. Demas, *J. Phys. Chem.*, 1971, **75**, 991–1024.
47 P. G. Seybold and M. Gouterman, *J. Mol. Spectrosc.*, 1969, **31**, 1–13.

Formatting – please delete this box prior to submission

- Graphics, including tables, will be located at the top or bottom of the column following their first citation in the text during production (unless they are equations, which appear in the flow of the text). They can be single column or double column as appropriate and require appropriate captions.
- Text is not wrapped around any of the graphics.
- During production, sufficient space will be inserted around graphics for clarity of reading; a horizontal bar will also be used to separate all inserted graphics, tables and their captions from the text:
- Please consult the Styles menu for recommended formatting for all text, including footnotes, references, tables, images and captions.